Journal of the Korean Magnetic Resonance Society **2010**, *14*, 55-75

DOI #: 10.6564/JKMRS.2010.14.2.055

Electron Spin Resonance Study of Manganese Ion Species Incorporated into Novel Aluminosilicate Nanospheres with Solid Core/Mesoporous Shell Structure

Gernho Back[1,*], Kiyub Kim[1], Yun Kyung Kim[2], and Jong-Sung Yu[2,*]

[1]*Department of Chemistry, Changwon National University, 9 Sarim-dong, Changwon, Kyungnam 641-773, Korea*
[2]*Department of Advanced Materials Chemistry. BK21 Research Team, Korea University, 208 Seochang, Jochiwon, 339-700, Korea*
(Received July 3, 2010; accepted Dec 9, 2010)

Abstract : An ion-exchanged reaction of $MnCl_2$ with Al-incorporated solid core/mesoporous shell silica (AlSCMS) followed by calcinations generated manganese species, where average oxidation state of manganese ion is 3+, in the mesoporous materials. Dehydration results in the formation of Mn^{2+} ion species, which can be characterized by electron spin resonance (ESR). The chemical environments of the manganese centers in Mn-AlSCMS were investigated by diffuse reflectance, UV-VIS and ESR spectroscopic methods. Upon drying at 323 K, part of manganese is oxidized to higher oxidation state (Mn^{3+} and Mn^{4+}) and further increase in (average) oxidation state takes place upon calcinations at 823 K. It was found that the manganese species on the wall of the Mn-AlSCMS were transformed to tetrahedral Mn^{3+} or Mn^{4+} and further changed to square pyramid by additional coordination to water molecules upon hydration. The oxidized Mn^{3+} or Mn^{4+} species on the surfaces were reversibly reduced to Mn^{2+} or Mn^{3+} species or lower valances by thermal process. Mn(II) species I with a well resolved sextet was observed in calcined, hydrated Mn-AlSCMS, while Mn (II) species II with g = 5.1 and 3.2 observed in dehydrated Mn-AlSCMS. Both species I and II are considered to be non-framework Mn(II).

Keywords : ESR, AlSCMS, Mn ion species, Mesopore, DRS, NMR

INTRODUCTION

* To whom correspondence should be addressed. E-mail : ghbaek@changwon.ac.kr; jsyu212@korea.ac.kr

Considerable interest in nanoporous materials such as zeolites and mesoporous molecular sieves stems from application potential such as catalysis, adsorption, and separation processes due to their well-developed ordered porous structures with high specific surface area, large pore volume, and narrow pore size distribution.[1-3] Amine molecules or surfactant micelles have been used as structure directing templates for the fabrication of the nanoporous materials.[4-8] These porous materials were mostly produced in amorphous powder type. Recently, porous materials with specific morphologies have attracted great attentions due to more specific applications.[9,10] Thus, the synthesis of tailored nanostructured particle has been a major challenge in advanced materials science. The focus mainly lies on understanding the formation mechanism of the nanostructured particles and on the conditions to tailor their particle morphology, particle size, and pore structure.[1] Many new nanostructured shell framework with either solid core or hollow core were generated depending on the removal of core templates.[9,10] Recently, sub-micrometer sized silica spheres with solid core and mesoporous shell (SCMS) structure were synthesized.[10-12] The core size and/or shell thickness of the SCMS particles can be controlled independently by two separate synthesis processes, consisting of solid core formation by the Stöber method (first step) and subsequent formation of the mesoporous shell by the Kaiser approach (second step).[13,14] Octadecyltrimethoxysilane (C_{18}-TMS) has been used as a porogen to generate the mesopores in the shell. The mesoporous silica layer on each silica particle was generated by co-hydrolysis and subsequent condensation of tetraethoxysilane and the C_{18}-TMS. The mesopores in the shell of the SCMS particles can be regulated with ordered or disordered

arrangement depending on the types of pore-generating surfactants.[8] Like all the mesoporous silica materials, the silica walls surrounding the SCMS spheres possesses an amorphous nature.[1,2] The incorporation of aluminum into the SCMS framework causes a negative net charge on the framework that is compensated by protons. Therefore, it is expected that aluminum-containing SCMS (AlSCMS) silica spheres can possess an ion-exchange capacity by other charge balancing cations such as paramagnetic transition metal ions as found in zeolite.[15,16] Such transition metal ion species in the AlSCMS system may offer potential for specially tailored catalytic applications.[17]

It is well-known that manganese oxide-loaded catalysts are useful as catalysts for various chemical reactions such as oxidation,[18-20] the catalytic combustion of methane[21] and volatile organic compound (VOC),[22] nitrous oxide decomposition[23] and ozone decomposition.[22] However, only a few papers have dealt with the local structural characteristics of the manganese metal ions in MCM-41[24-28] and silica spheres with shell consisting of ordered mesoporous structure similar to MCM-41 hexagonal structure.[29] There has been little study about the structure and application of Mn species in mesoporous materials with structurally important morphology despite their importance in catalysis and adsorption. The potential catalytic application of the metal ion sites requires detailed characterization of their environment in the mesoporous materials including their framework position and coordination structure.

In this work, Mn ion species were exchanged for the first time into the mesoporous non-framework through solid-state reaction of $MnCl_2$ with the AlSCMS nanosphere to form Mn-AlSCMS.

Interestingly, the AlSCMS silica spheres possess disordered mesoporous structure in the shell as C_{18}-TMS has been used as a porogen to generate the mesopores in the shell. The paramagnetic Mn species generated by thermal reduction were characterized using electron spin resonance (ESR), fourier transform(FT)-infrared(IR) and diffuse reflectance spectroscopy(DRS) in ultraviolet(UV)-visible(Vis)-near IR region to gain information about the coordination of the Mn species. This study illustrates that Mn ion species in reduced Mn-AlSCMS by H_2 exists in a non-framework position.

EXPERIMENTAL

Synthesis of SCMS aluminosilicate spheres

SCMS silica was synthesized according to literature.[10-12] The following procedure describes the synthesis of the SCMS silica spheres with a core diameter of 180 nm and a shell thickness of 50 nm. About 3.14 ml of aqueous ammonia (32 wt%) was added to a solution containing 74 ml of ethanol and 10 ml of deionized water. 6 ml of tetraethoxysilane (TEOS) was added to the above-prepared mixture at 303 K with vigorous stirring, and the reaction mixture was stirred continuously for 1 h to yield uniform silica spheres (Stöber silica solution). A mixture solution containing 5 ml of TEOS and 2 ml of octadecyltrimethoxysilane (C_{18}-TMS) (90%, Aldrich) (i.e., molar ratio of TEOS to C_{18}-TMS = 4.7) was added to the colloidal solution containing the silica spheres and further reacted for 1 h. The resulting octadecyl group incorporated silica particles were retrieved by centrifugation, and

further calcined at 823 K for 6 h under an oxygen atmosphere to produce the final solid core/mesoporous shell (SCMS) silica material. Aluminum was incorporated into the silicate framework through an impregnation method. A total of 0.3 g of the SCMS silica was added into an aqueous solution containing 0.078 g of $AlCl_3 \cdot 6H_2O$ in 20.0 ml of water, and the resulting slurry was stirred at 393 K for 6 h. The material was heated with increasing temperature under stirring condition in order to vaporize water. The material was then washed at 343 K in deionized water in order to remove any ions adsorbed on the external surface. The powder was dried in air at 353 K. Finally, the Al-impregnated SCMS silica was calcined at 823 K for 5 h in air to yield SCMS aluminosilicate (AlSCMS). $CaCl_2$-exchanged sample. was obtained by stirring 0.5 g of calcined AlSCMS in 50 ml of 0.05 M $CaCl_2$ solution at 333 K for 2 h. This procedure was done twice. The resulting sample is denoted by AlSCMS(Ca). Some non-framework Al in AlSCMS (Ca) was detected by solid state MAS NMR.

Synthesis of Mn-AlSCMS

Mn-AlSCMS material was prepared by a procedure similar to the procedure for Mn-AlMCM-41.[30] Mn(II) ion-exchanged sample was prepared by overnight stirring. This material was then filtered and washed at 343 K in deionized water in order to remove any ions adsorbed on the external surface. The ion-exchanged sample is denoted by Mn-AlSCMS.

Sample Treatment and Measurements

N_2 adsorption and desorption isotherms were measured at 77 K on a KICT SPA-3000 Gas Adsorption Analyzer after the sample was degassed at 423 K to 20 μTorr for 12 h. The specific surface areas were determined from nitrogen adsorption using the Brunauer-Emmett-Teller (BET) equation. Total pore volume was determined from the amount of gas adsorbed at the relative pressure of 0.99. Pore size distribution (PSD) was derived from the analysis of the adsorption branch using the Barrett-Joyner-Halenda (BJH) method.

Powder X-ray diffraction (XRD) patterns were recorded on a Phillips PW 1840 X-ray diffraction using CuKα radiation with a wavelength 1.541 Å. Chemical analysis of the samples was carried out with Oxford Energy dispersive X-ray spectrometer. The MAS-NMR spectra were recorded at 9.4 T using a Bruker DSX600 solid-state NMR spectrometer. ^{27}Al-MAS spectra were measured at 104.18 MHz using a π /20 pulse and a recycle delay time of 1 s. The 4 mm rotor was spun at a frequency of 13.2 kHz. External $AlCl_3$ was used as a chemical shift reference. Ammonia-TPD (temperature programmed desorption) was performed with gas chromatography (Micromertex Autopure 2920) attached with TCD (thermal conductive detector). The AlSCMS and SCMS samples were filled into the quartz tube and finally connected in the vacuum line on-lined with gas chromatography. The samples were activated in situ at 573 K for 3 h in the presence of high-purity helium with a flow rate of 140 ml/min to remove physically adsorbed water and then cooled to 298 K. The samples subsequently were adsorbed with NH_3 at 373 K for 2 h. NH_3-TPD was performed at the region of 373

K-1073 K with the heating rate 278 K/min. The diffuse reflectance (DR) UV-Vis spectra were recorded using a Varian model Cary 1C spectrometer with an integrating sphere accessory.

ESR spectra were recorded with 300 MHz spectrometer (Jeol model JES-FA) at 77 K and 298 K using 3 mm o.d. x 2 mm i.d. Suprasil quartz tube. Magnetic field was calibrated with a Jeol model ES-FCB gauss meter. The as-synthesized Mn-AlSCMS was first evacuated to a final pressure of 10^{-4} Torr and then heated under vacuum from 295 K to 623 K at regular intervals to study the behavior of the Mn species as a function of the dehydration. The temperature was raised slowly and held at several temperatures, each for 5 ~ 15 h. ESR spectra were measured at 77 K to observe the change of the Mn species in the Mn-AlSCMS. To study the redox behavior of the Mn species, the dehydrated sample at 573 K was contacted with atmosphere of O_2 at room temperature(RT) for 2 min and then evacuated at same temperature briefly for 1 min to remove physically attached oxygen. Upon reduction at 573 K by atmosphere of H_2 the near-IR DRS spectrum was measured with Jasco V-670 spectrophotometer. FT-IR spectra were recorded with Nicolet Impact 410 DSP spectrometer using KBr pellets coupled to an AT-386 SX computer.

RESULTS AND DISCUSSION

Characterization of AlSCMS

Fig. 1a and b show the scanning electron microscopic (SEM) and transmission electron microscopic (TEM) images of the AlSCMS. The SEM image reveals that the particles are spherical and uniform with diameters of ~ 280 nm and no agglomeration takes place. The TEM image shows clearly a 180 nm sized core and a 50 nm thick mesoporous shell. The mesopores were randomly distributed over the shell, whereas the core was dense and non-porous. Some particles are deformed, and this deformation seems to be the result of mechanical stress during the thermal removal of octadecyl groups incorporated in the silica particles.

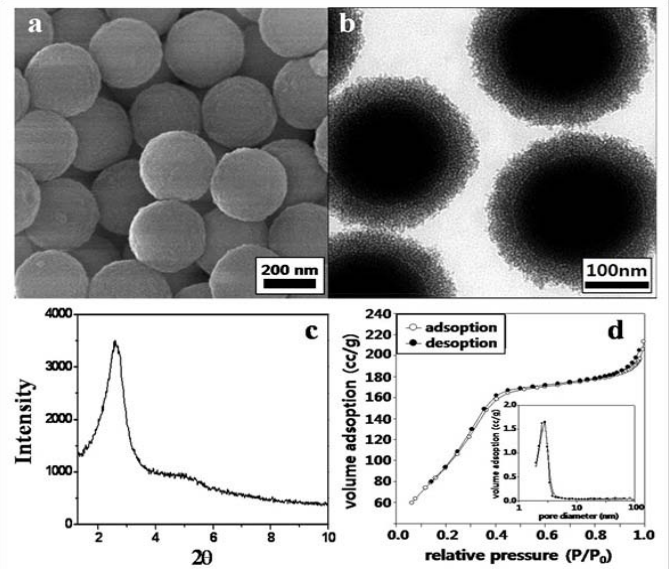

Figure 1. a) SEM and b) TEM images of AlSCMS with a core diameter of 180 nm and a shell thickness of 50 nm. c) XRD pattern of the AlSCMS. d) Nitrogen sorption isotherms at 77 K for calcined AlSCMS and pore size distribution determined by BJH method(insert).

XRD patterns of the AlSCMS are shown in Fig. 1c. The XRD pattern similar to hexagonal-type mesoporous structure despite being rather poorly resolved could be obtained with a d-spacing of ca. 3.3 nm. The unit cell parameter (a_0) was calculated to be 3.8 nm on the basis of $2d_{100}/\sqrt{3}$ from d_{100}

which is obtained from 2 θ of the first peak in the XRD pattern by Bragg's equation[29] ($2d\sin\theta = \lambda$, λ = 1.541 Å for the Cu Kα line). Chemical analysis of the AlSCMS samples was carried out with Oxford Energy dispersive X-ray spectrometer. The ratio for Si/Al is found to 11.0.

Typical nitrogen sorption isotherms at 77 K and the corresponding pore size distribution are shown in Fig. 1d. The nitrogen isotherms indicate a linear increase of the amount of adsorbed nitrogen at low pressures (less than p/p_0 = 0.25), and a hysteresis between the adsorption branch and the desorption branch appears. The resulting isotherm can be classified as a type IV isotherm with H2-type hysteresis according to the IUPAC nomenclature. The steep increase in nitrogen uptake at relative pressures in the range between p/p_0 = 0.3 and 0.50 is reflected in a narrow pore size distribution. The pore size from the PSD maximum was estimated as ca. 2.4 nm with a narrow PSD. The AlSCMS exhibits specific surface area of ca. 396 m^2/g and total pore volume of ca. 0.32 cm^3/g, which are mainly attributable to the presence of the mesopores in the shell. From the unit cell parameter a_0, which is equal to one internal pore diameter plus one pore wall thickness, the wall thickness is determined to be 1.4 nm.

^{27}Al MAS NMR

^{27}Al MAS NMR spectroscopy was used to confirm the incorporation of aluminum into the framework of as-synthesized SCMS silica particles. The ^{27}Al MAS NMR spectrum of the sample in Fig. 2 gives a single sharp resonance at 56.2 ppm from Al in tetrahedral (framework) coordination. In

addition, less intense lines are also obtained at ca. 30 and -1.4 ppm corresponding to octahedral coordination, which indicates a non-framework Al species. A rough estimation of the intensity of the lines corresponding to the non-framework Al species compared to the intensity of the line at 56.2 ppm shows that about 99 % of the Al species are framework species.

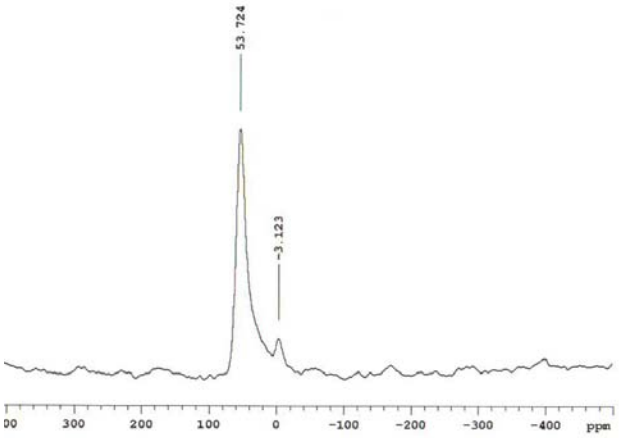

Figure 2 .[27]AlSCMS NMR spectrum of calcined AlSCMS The spectrum is in good agreement with the previous data[30-34], indicating it is not likely that the non-framework aluminum affects the location of Mn ion species.

Ammonia-TPD

The substitution of some silicone by aluminum in the framework of SCMS also generates acid sites in the framework. NH_3-TPD was used to confirm the acid sites. The TPD signals at 200 ^oC and 400 ^oC in the AlSCMS sample were four and two times higher than those of the SCMS, respectively

as shown in Fig. 3. The comparison of the curves on Figures 3a and 3b leads to a conclusion that at 400 ^{o}C AlSCMS sample has more strong acid sites than SCMS one due to the presence of framework Al of the former. The signal occurring at lower temperature of 200 ^{o}C can be assigned to non-framework Al species.

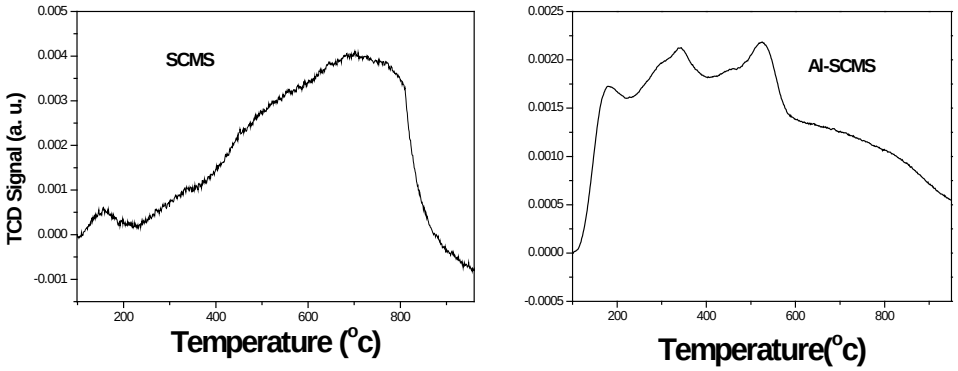

Figure 3. NH_3-TPD profile for the sample of (a) SCMS and (b) AlSCMS desorbed at heating rate 5℃/min.

ESR investigation

To study the redox behavior of Mn-AlSCMS, as-synthesized Mn-AlSCMS was dehydrated by slowly raising the temperature from room temperature (RT) to 623 K. The ESR spectra of the Mn-AlSCMS samples before and after various treatments were measured and shown in Fig. 4. The as-synthesized Mn-AlSCMS before dehydration produced six hyperfine lines centered on g = 2.00 with line-width ΔH_{pp} = 96 G at 77 K. The lines corresponding to forbidden transitions appear between the

allowed sextet lines. The observation of forbidden transitions indicates mixing with zero magnetic field transitions that are not averaged by motion of the Mn(II) complex, hence illustrating an immobile Mn(II) species at 77 K.[31-33] The sextet lines are not equally spaced in Fig. 4. The peak-to-peak line-width increases and the line height decreases. The average hyperfine coupling constant A_{iso} from Fig. 4 is 96 G. Only one Mn(II) species seems to exist in Mn-AlSCMS. These ESR parameters indicate that this Mn(II) species has octahedral coordination[34,35], which is consistent with an extra-framework positions.[34,35]

Dehydration and rehydration of Mn-containing AlSCMS materials

ESR was used to study the dehydration and rehydration behavior of Mn-AlSCMS as shown in Fig. 4. Before dehydration, only Mn(II) species I is observed. During dehydration from RT to 623 K, Mn(II) species I is still well resolved with almost the same g and A values as shown in Fig. 4(a-c). Only its peak-to-peak line-width becomes broader from 12 G to 18 G in Fig. 4 (c). Two new low field peaks around g = 5.2 and 3.2 are detected after evacuation at 393 K as seen in Fig. 4 (b) and at 623 K in Fig. 4(c) which are assigned to Mn(II) species II. After D_2O is absorbed on dehydrated Mn-AlSCMS at 293 K for 30 min, complete rehydration occurs, and the low field peaks all disappear while the original Mn(II) species I was recovered as before dehydration for 14 h. Although peak intensity was slightly weakened, not much significant change in the ESR spectrum was observed.

Table 1. ESR parameter of Mn-containing reference compounds.

Mn^{n+}	loading	environments	symmetry	g, A	ref
Mn^{2+}	1-6%	γ-Al_2O_3	T_d/O_h	$g_\perp$=2,00, $A_\perp$=76.6 G	30
Mn^{4+}	0.1%	MgO-LiO	axial	$g_\perp$=1.995, $A_\perp$=70.0 G	30
Mn^{2+}	0.05 mol%	AlMCM-41 site I site II	distorted T_d distorted O_h	$g_\perp$=2.007, $A_\perp$= 97 G $g_{//}$=3.2, 5.2 $g_\perp$=2.007 $A_\perp$=97 G	30
Mn^{2+},Mn^{4+}	11wt%	AlSCMS	distorted O_h	$g_{//}$ = 3.2, 5.1 $g_\perp$=2.00, $A_\perp$=76 G	TW

This Work(TW)

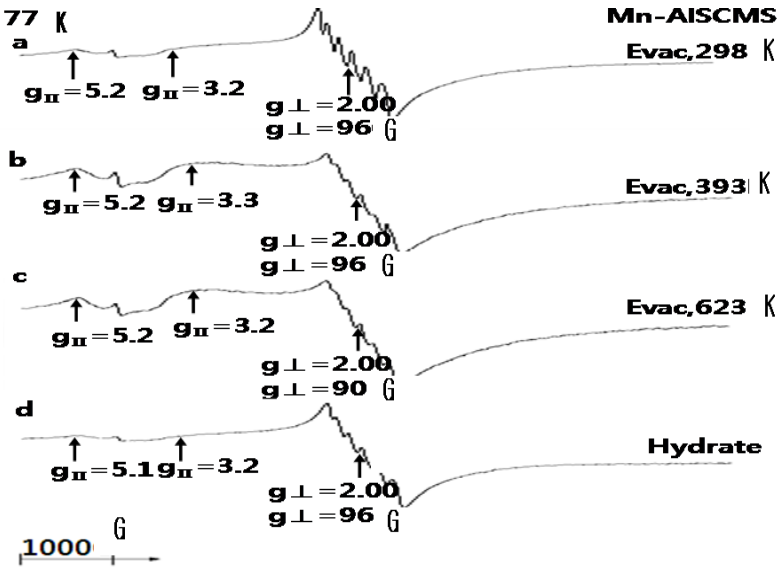

Figure 4. ESR spectra at 77 K of Mn-AlSCMS after evaluation for ~ 15 h a) at RT, b) at 393 K, c) at 623 K, and d) after rehydration with D_2O at RT following dehydration for 15 h at 623 K under vacuum.

Diffuse Reflectance Spectroscopy

Dried and Calcined Samples. The DRS spectrum of the freshly calcined 2 wt% Mn-AlSCMS is shown in Figure 5. The absorption bands appeared at around 18000 cm^{-1} and 21000 cm^{-1}, which are

assigned to charge transfer from O^{2-} to $Mn^{2+,4+}$. Moreover, the first overtone (2 ν) of molecularly adsorbed water (6800 cm^{-1}) can be seen, accompanied by a combination band (ν + δ) at 5250 cm^{-1}, as shown in Figure 6.[36]

Upon calcinations at 823 K, the intensity of the Mn band centered at 21000 cm^{-1} has increased considerably, and a weak shoulder around 25000 cm^{-1}.[37] The surface hydroxyls are well pronounced at 7210 and 7290 cm^{-1}, as shown in Figure 7, which were assigned to the overtones of acidic and neutral hydroxyls, respectively.[37]

Up to 8 wt% loading, the intensity of Mn band increases with loading. It should be mentioned that at higher loading, the Kubelka-Munk law is no longer valid. DRS study shows the same phenomena observed in Al_2O_3 within similar Mn quantity.[38]

Reduced sample. During reduction, the color of the sample progressively changes from the pale pink to brown. The spectral change of the Mn band of 2 wt% Mn-AlSCMS during reduction by H_2 is shown in Fig. 8. Before reduction, the sample was dehydrated in O_2 at 573 K: the spectrum shows a band in the range of 21500 -22800 cm^{-1}. Moreover, a very weak feature is observed around 25000 cm^{-1}. Upon reduction at 573 K, the entire spectrum is considerably less intense. The maximum of band 2 is slightly more pronounced. The maximum of band 1 is shifted slightly upward. DRS study also shows similar result in Al_2O_3 within similar Mn quantity.[38]

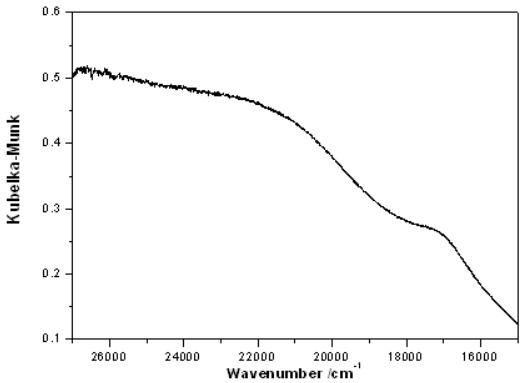

Figure 5. DRS spectrum of 2 wt% Mn-AlCMS after drying at 363 K followed by calcinations in O_2 at 823 K.

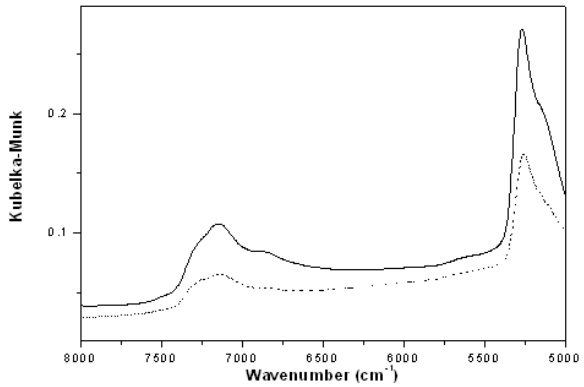

Figure 6. DRS spectra of samples with 8 wt % (---) and 15 wt % (—) for Al/Al+Si after calcinations at 823 K.

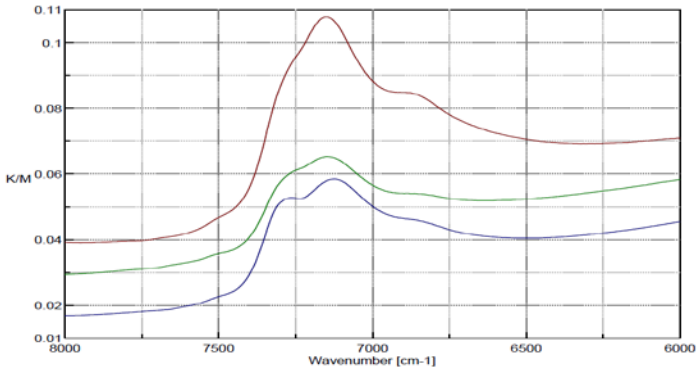

Figure 7. DRS spectra of SCMS-supported Manganese oxide after calcination in O_2 at 823 K; (a) 2% Mn (b) 4% Mn (c) 8% Mn.

Table 2. Absorption maximum of d-d transitions of Mn-containing reference compounds

Mn^{n+}	environments	Abs max/cm^{-1}	transion	ref
Mn^{2+}	MnO	16400 20800 23800	$^4T_2 \leftarrow {}^6A_1$ $^4T_2 \leftarrow {}^6A_4$ $^4A_1 \leftarrow {}^6A_1$	41
Mn^{3+}	Mn-APO-34	20400	$^5T_{2g} \leftarrow {}^5E_g$	42
Mn^{4+}	Al_2O_3	21300	$^4T_{2g} \leftarrow {}^4A_{2g}$	43
Mn^{2+},Mn^{4+}	AlSCMS	18000 21000	$^5T_{2g} \leftarrow {}^5E_g$	TW

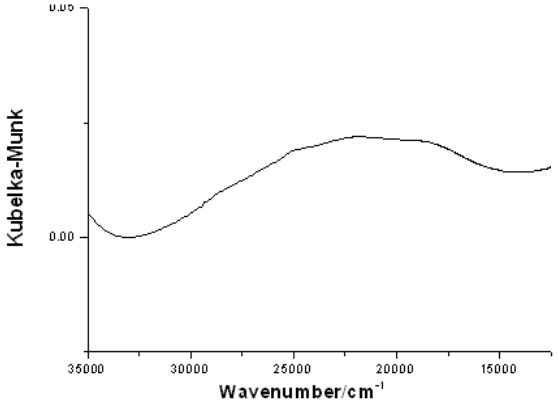

Figure 8. DRS spectrum of 2 wt% Mn-AlSCMS after calcination at 823 K and reduction by H_2 at 573 K during 5 h.

FT-IR spectrum

The FT-IR spectrum of the Mn-AlSCMS samples is shown in Figure 9b along with that of the reference material, AlSCMS. The Mn-O stretching bands are observed in the 950-700 cm^{-1} range,[39] while the Al-O stretching and deformation modes are in the 600-400 cm^{-1} range.[40,41] An absorption peak at 663 cm^{-1} appeared after calcinations at 550 ^oC for 5 h of as-synthesized Mn-AlSCMS is assigned to a Mn-O band. Unfortunately, the other absorption bands near at the 460 cm^{-1} corresponding to the Mn-O stretching band could not be identified because they are expected to appear at absorption band similar to those of Al-O modes and silica framework.[42] It is reasonable to assign the absorption peak at 663 cm^{-1} to the asymmetrical Mn-O stretching band.

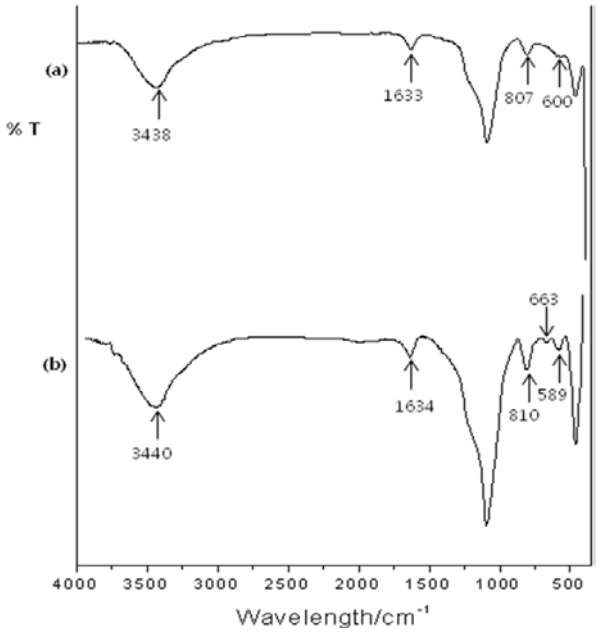

Figure 9. FT-IR spectra of a) reference AlSCMS and b) Mn-AlSCMS, both of which are calcined at 550 ^{o}C for 5 hrs.

Reaction Scheme for the Preparation of Mn-AlSCMS.

The $Mn(H_2O)_6$ complex is the precursor molecule present in an aqueous solution of manganese chloride. During impregnation and subsequent drying, the reaction of this complex with both acidic and basic hydroxyls of the AlSCMS support can be presented as shown in Fig. 10.

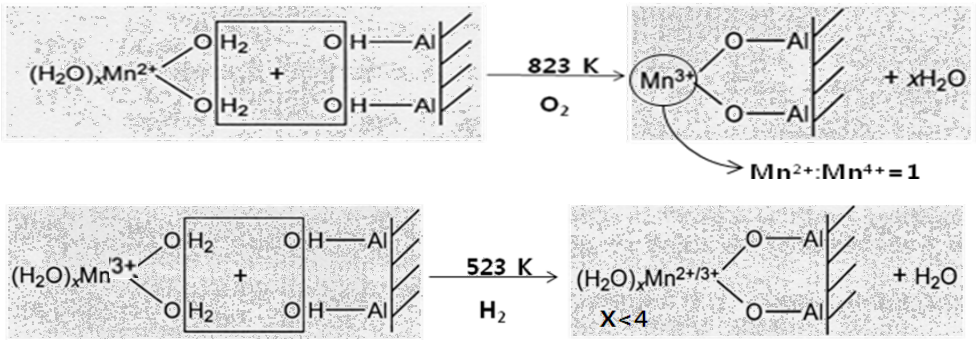

Figure 10. The reaction of $Mn(H_2O)_6$ complex with hydroxyls of the AlSCMS support for the preparation of Mn-AlSCMS.

CONCLUSIONS

On the basis of investigations made by ESR and DRS of AlSCMS-supported manganese oxide, the following conclusions can be drawn: during impregnation of the aqueous solution, the $Mn(H_2O)_6]^{2+}$ complex reacts with the surface hydroxyl of AlSCMS supports. At loading above approximately 8 wt%, the reaction with hydroxyl is accompanied by deposition of the complex

The part of manganese was oxidized to higher oxidation state upon during at 383 K, while a increase in average oxidation state takes place during further calcinations at 823 K. The manganese oxide obtained are present as a mixture, where Mn^{2+} and Mn^{4+} are present in a 1/1 ratio. Dehydration results in the formation of a paramagnetic manganese ion species that can be characterized by ESR.

From the ESR study on Mn-AlSCMS , two species I and II are found and assigned to non-framework species. Species I at g = 2.007 exists at hydrated non-framework positions as distorted octahedral Mn(II) ion. Species II at g = 5.2 and 3.2 is assigned to distorted tetrahedral non-framework Mn(II) ion.

Acknowledgment

This research was financially supported by the Changwon National University in 2009 and the Korea Institute for Advancement of Technology (KIAT-2009) through the Human Resource Training Project for Regional Innovation. G. Back and JSYu thanks KBSI at Daegu, Jeonju and Daejeon for the ^{27}Al MAS NMR, SEM and TEM measurements.

REFERENCES

1. J.S Beck, J.C. Vartuli, W.J. Roth, M.E. Leonowicz, C.T. Kresge, K.D. Schmitt, CT-W. Chu, D.H. Olson, E.W. Scheppard, S.B. McCullen, J.B. Higgins, J.L. Schlenker, *J. Am. Chem. Soc*. **114**, 10834. (1992).
2. C.T. Kresge, M.E. Leonowicz, W.J. Roth, J.C. Vartuli, J.S. Beck, *Nature* **359**, 710. (1992).
3. C.-Y. Chen, S.L. Burkett, H.-X. Li, M.E. Davis, *Microporous Mater*. **2**, 27. (1993).
4. S.B. Yoon, J.Y. Kim, J.-S. Yu, *Chem. Commun*. **1536**. (2002).
5. J.Y. Kim, S.B. Toon, F. Koli, J.-S. Yu, J. *Mater. Chem.* **11**, 2912. (2001).
6. A. Vinu, C. Streb, V. Murugesan, M. Hartman, *J. Phys. Chem*. **B 107**, 8297. (2003).
7. S.B. Yoon, J.Y. Kim, J.-S. Yu, *Chem. Commun*. **1740**. (2003).
8. S.B. Yoon, J.Y. Kim, J.H. Kim, Y.J. Park, K.R. Yoon, S.K. Park, J.-S. Yu, J. *Mater. Chem.* **17**, 1758. (2007).
9. H. Zhang, Sun, J.D. Ma, G. Weinberg, D.S. Su, X. Bao, *J. Phys. Chem.* **B 110**, 25908. (2006).

10. A. Vinu, D.P. Sawant, K. Ariga, K.Z. Hossain, S.B. Halligudi, M. Hartmann, M. Nomura, *Chem. Mater.* **17**, 5339. (2005).

11. S.B. Yoon, K. Sohn, J.Y. Kim, C.-H. Shin, J.-S. Yu, T. Hyeon, *Adv. Mater*. **14**, 19. (2002).

Q. Ji, S. Achaya, J. P. Hill, A. Vinu, S. B. Yoon, J.-S. Yu, K. Sakamoto, K. Anga, *Adv. Funct. Mater.* **199**, 1792. (2009).

12. W. Stöber, A. Fink, E. Bohn, *J. Colloid Interface Sci.* **26**, 62. (1968).

13. C. Kaiser Ph.D. *Thesis, Johannes Gutenberg-Universitat Mainz, Germany* (1996).

14. L. Kevan, *Acc. Chem. Res.* **20**, 1. (1987).

15. A. Pŏple, M. Newhouse, L. Kevan *J. Phys. Chem*. **99**, 10019. (1995).

16. J.E. Maxwell, *Adv. Catal*. **31**, 1. (1982).

17. M.A. Baltanás, A.B. Stiles, J.R. Katzer, *Appl. Catal.* **28**, 13. (1986).

18. N.I. II'Chenko, G.I. Godolets, *J. Catal*. **39**, 57. (1975).

19. H.T. Karlsson, H.S. Rosenberg, *Ind. Eng. Chem. Process Res. Dev*. **23**, 808. (1984).

20. D. Van der Kleut Ph. D. *Thesis, University of Utrecht, The Nethelands* (1994).

21. A. Nishino, *Catal. Today*. **10**, 107. (1991).

22. M. Lo Jacono, M. Schiavello, Preparation of Catalysts, B. Delmon, P.A. Jacobs, G. Poncelet Eds *Elsevier, Amsterdam* p. 474 (1976).

23. A. Pöpple, P. Baglioni, L. Kevan, *J. Phys. Chem*. **99**, 14156. (1995).

24. A. Pöpple, L. Kevan, *Langmuir* **11**, 4486. (1995).

25. A. Pöpple, M. Hartmann, L. Kevan, *J. Phys. Chem*. **99**, 17251. (1995).

26. V. Luca, D.J. MacLachlan, R. Bramley, K. Morgan, *J. Phys. Chem*. **100,** 1793. (1996).

27. a. M. Hartmann, A. Poppl, L. Kevan, *J. Phys. Chem*. **99**, 17494 (1995). b. G. Breuet, X. Chen, C. W. Lee, L. Kevan, *J. Am. Chem. Soc*. **114**, 3720. (1992).

28. a G. Back, H. Lee, M. Kim, J.-S. Yu, S. Jeong , Y. B. Chae, *J. Mater. Sci*. **44**, 5636 (2009) b B.

29. D. Cullity, Elements of X-ray diffraction, Addison-Wesley, *Reading, MA*, p. 87 (1987).

30. J. Xu, Z. Luan, T. Wasowicz, L. Kevan, *Micro Mesoporous Mater*. **22**, 179. (1998).

31. D.Y. Zhao, D. J. Goldfarb, *Chem. Soc. Chem. Commun.* **875**. (1995).

32. D.Y. Zhao, D.J. Goldfarb,In: L. Bonneviot, S. Kaliaguine, (Eds) Zeolites: A Refined Tool for Designing Catalytic Sites, *Elsevier, Amsterdam* pp 181-188. (1995).

33. E. Meirovitch, R. Poupko, *J. Phys. Chem.* **82**, 1920. (1978).

34. G. Brouet, X. Chen, C.W. Lee, *J. Am. Chem. Soc.* **114**, 3720. (1992).

35. Z. Levi, Gaitsimiring, D.J. Goldfarb, *J. Phys. Chem*. **95**, 7830. (1991).

36. R. A. Scoonheydt, F. Delannay, E. d. Dekker, *New York*. P. 125. (1984).

37. H. Knozinger, D. Ratnasamy , *Catal. Rev.-SCi. Eng.***17**, 31. (1978) .

38. W. Sjoerd Kijstra. Eduard K. Poels, Alfred Bliek, Bert M. Weckhuysen, and Robert A. Schoonheydt, *J. Phys. Chem. B* **101**, 309. (1997).

39. a Raluca Ciceo Lucacel, Carmen Marcus, V. Timar, I. Ardelean, *Solid State Sciences* **9**, 850. (2007). b S. R. G. Carrazan, C. Martin, V. Rives, R. Vidal, *Spectrochimia Acta A*, **52**, 1107. (1996). c R.J. Keller, *Sigma Chemical Co. Inc*, **2,** 1039. (1985) .

40. G.W. Pratt, R. Coelho, *Phys. Rev.* **116**, 381. (1959).

41. M. Rjic, D. Stejakovic, S. Hocevar, V. Kaueic, *Zeolites* **13**, 3849. (1993).

42. S. Geschwind, M.P. Kisliuk, J.P. Remeika, D.L. Wood, *Phys. Rev*. **136**, 1684. (1962).